Turkish Journal of Electrical Engineering & Computer Sciences

http://journals.tubitak.gov.tr/elektrik/

Research Article

Turk J Elec Eng & Comp Sci
(2014) 22: 1056 – 1075

doi:10.3906/elk-1204-1

A novel hybrid recurrent wavelet neural network control of permanent magnet synchronous motor drive for electric scooter

Chih-Hong LIN*
Department of Electrical Engineering, National United University, Miaoli, Taiwan

Received: 01.04.2012 • **Accepted:** 23.07.2012 • **Published Online:** 17.06.2014 • **Printed:** 16.07.2014

Abstract: Due to the electric scooter with nonlinear uncertainties, e.g., nonlinear friction force of the transmission belt, the linear controller was made to disable speed tracking control. In order to overcome this problem, a novel hybrid recurrent wavelet neural network (NHRWNN) control system is proposed to control for a permanent-magnet synchronous motor-driven electric scooter in this study. The NHRWNN control system consists of a supervised control, a recurrent wavelet neural network (RWNN), and a compensated control with adaptive law. According to the Lyapunov stability theorem and the gradient descent method, the on-line parameter training methodology of the RWNN can be derived by using adaptation laws. The RWNN with the on-line learning ability can respond to the system's nonlinear and time-varying behaviors according to different speeds in the electric scooter. The electric scooter is operated to provide disturbance torque with nonlinear uncertainties. Finally, performance of the proposed NHRWNN control system is verified by experimental results.

Key words: Permanent magnet synchronous motor, recurrent wavelet neural network, electric scooter

1. Introduction

For the purpose of reducing petroleum dependence and air pollution, there are many countries developing electric vehicles for substitution of the petroleum-power supply. Because scooters are much more extensive than cars for personal transportation in Taiwan, I have been studying the development and research of the electric scooter. Because the wheels of the electric scooters are driven by AC motor, the selection of the AC motor drive system is a very important job. The AC servo motors have been widely used in many applications of mechatronics, e.g., robotics, elevators, and computer numerical control [1,2]. There are several basic types for the AC servo motors, such as permanent magnet synchronous motors (PMSMs), switched reluctance motors (SRMs), and induction motors (IMs). The PMSMs provide higher efficiency, higher power density, and lower power loss for their size compared to SRMs and IMs. Field-oriented control is the most popular control technique used with PMSMs. As a result, torque ripple can be extremely low, on par with that of SRMs and IMs. On the other hand, PMSMs are controlled by field-oriented control, which can be achieved by fast 4-quadrant operation, and are much less sensitive to the parameter variations of the motor [1–3]. Therefore, they are often used in the design of AC servo drives.

The feedforward neural networks (NNs) have been extended successfully to applications in system identification and control in the past several years [4–10]. It has been proven that NNs can approximate a wide range of nonlinear functions. However, it is more difficult to obtain sensitivity information for highly nonlinear

*Correspondence: jhlin@nuu.edu.tw

dynamics. Wavelets have been combined with the NN to create wavelet neural networks (WNNs). This combines the capability of artificial NNs for learning from the process with the capability of wavelet decomposition for identification and control of dynamic systems [11–24]. The training algorithms for WNNs typically converge in a smaller number of iterations than that used for conventional NNs. Unlike the sigmoid functions used in conventional NNs, the second layer of a WNN is of a wavelet form, in which the translation and dilation parameters are included. Thus, the WNN has been proven to be better than the other NNs, since its structure can provide more potential to enrich the mapping relationship between inputs and outputs [12,13]. The WNN-based controllers combine the capability of NNs for on-line learning ability and the capability of wavelet decomposition for identification ability. Thus, the WNN-based controllers have been adopted widely for the control of complex dynamical systems and dynamic plants [14–24]. Such NNs are static input/output mapping schemes that can approximate a continuous function to an arbitrary degree of accuracy.

A recurrent NN (RNN) [25–29] based on supervised learning is a dynamic mapping network and is more suitable for describing dynamic systems than the NN. For this ability to temporarily store information, the structure of the network is simplified. The recurrent WNN (RWNN) [30,31] combines the properties of attractor dynamics of the RNN and the good convergence performance of the WNN. In [30,31], the RWNN was shown to deal with time-varying input or output through its own natural temporal operation due to internal feedback neurons in the input layer. It can then capture the dynamic response of a system.

Due to real plants with many nonlinear dynamics, e.g., electric scooter [32m33], the hybrid recurrent fuzzy neural network (RFNN) controller may not provide satisfactory control performance when operated over a wide range of operating conditions. In [32], the hybrid RFNN controller using rotor flux estimator controlled the PMSM without a shaft encoder to drive an electric scooter. The rotor flux estimator, which consists of the estimation algorithm of rotor flux position and speed based on the back electromagnetic force, is developed to provide rotor position for feedback control. The favorable speed tracking responses can be achieved by using the hybrid RFNN controller at 1200 rpm, but poor speed tracking responses are seen at 2400 rpm due to high speed perturbation. In [33], the hybrid RFNN control was feedback control for a PMSM-driven electric scooter with shaft encoder. The favorable speed tracking responses could only be achieved by using the hybrid RFNN controller at 1200 rpm in the nominal case and the parameter variation case. On the other hand, if the controlled plant has highly nonlinear uncertainties, the proportional-integral (PI) and proportional-integral-derivative (PID) controllers may also not provide satisfactory control performance. Therefore, to ensure the controlled performance of robustness, a PMSM controlled by a novel hybrid RWNN (NHRWNN) control system is developed to drive an electric scooter in this paper. A NHRWNN control system has fast learning properties and good generalization capability. The control method, which is not dependent upon the predetermined characteristics of the motor, can adapt to any change in the motor characteristics. A NHRWNN control system, which is composed of a supervised control, a RWNN, and a compensated control with adaptive law, is applied to a PMSM drive electric scooter system. The on-line parameter training methodology of the RWNN can be derived by using adaptation laws according to the Lyapunov stability theorem. The RWNN has the on-line learning ability to respond to the system's nonlinear and time-varying behaviors according to different speeds in the electric scooter. Finally, the performance of the proposed NHRWNN control system is verified by experimental results.

1.1. Configuration of field-oriented PMSM drive system

For convenient analysis, the voltage equations of a PMSM can be described in the rotor rotating reference frame as follows [1–3,32,33]:

$$v_{q1} = R_1 i_{q1} + L_{q1}\dot{i}_{q1} + \omega_1 L_{d1} i_{d1}, \tag{1}$$

$$v_{d1} = R_1 i_{d1} + L_{d1}\dot{i}_{d1} - \omega_1 L_{q1} i_{q1}, \tag{2}$$

in which v_{d1} and v_{q1} are the $d-$ and q-axis stator voltages, i_{d1} and i_{q1} are the $d-$ and q-axis stator currents, L_{d1} and L_{q1} are the $d-$ and q-axis stator inductances, R_1 is the stator resistance, and ω_1 is the rotor speed. The electromagnet torque T_m of a PMSM drive electric scooter can be described as:

$$T_m = \frac{3}{2}\frac{P_1}{2}\left[L_{m1} I_{fd1} i_{q1} + (L_{d1} - L_{q1}) i_{d1} i_{q1}\right]. \tag{3}$$

The equation of the motor dynamics is:

$$T_m = T_{L1} - B_1\omega_1 + J_1\dot{\omega}_1, \tag{4}$$

where P_1 is the number of poles; T_{L1} is the external load disturbance, e.g., the electric scooter; B_1 represents the total viscous frictional coefficient; and J_1 is the total moment of inertia. The control principle of the PMSM drive system is based on field orientation. Due to $L_{d1} = L_{q1}$ and $I_{d1} = 0$ in the surface-type PMSM, the second term of Eq. (3) is 0. Moreover, L_{m1} and I_{fd1} are constants for a field orientation control of the surface-type PMSM. The electromagnetic torque T_m is a function of i_{q1}. The electromagnetic torque T_m is linearly proportional to q-axis current i_{q1}. When the d-axis rotor flux is constant, the maximum torque per ampere can be reached for the field-oriented control at the T_m proportional to the i_{q1}. The PMSM drive with the implementation of field-oriented control can be reduced to:

$$T_m = K_e i_{q1}^*, \tag{5}$$

$$K_e = 3P_1 L_{m1} I_{fd1}/4. \tag{6}$$

The block diagram of a PMSM drive electric scooter system is described in Figure 1. The whole system of a PMSM drive electric scooter can be indicated as: a field-oriented institution, a current PID control loop, a sine PWM control circuit, interlock and isolated circuit, an IGBT power module inverter, and a speed control loop [31,32]. The current PID loop controller is the current loop tracking controller. The control gains K_P, K_I, and K_D of the PID loop controller are $K_P = 15, K_I = 2, K_D = 0.5$ to attain good dynamic response by using the trial-and-error method. The field-oriented institution consists of the coordinate transformation, $\sin(\theta_f)/\cos(\theta_f)$ generation, and lookup table generation. We use the TMS320C32 DSP control system to implement field-oriented institution control and speed control. The PMSM drive electric scooter is manipulated at load disturbance torque with nonlinear uncertainties.

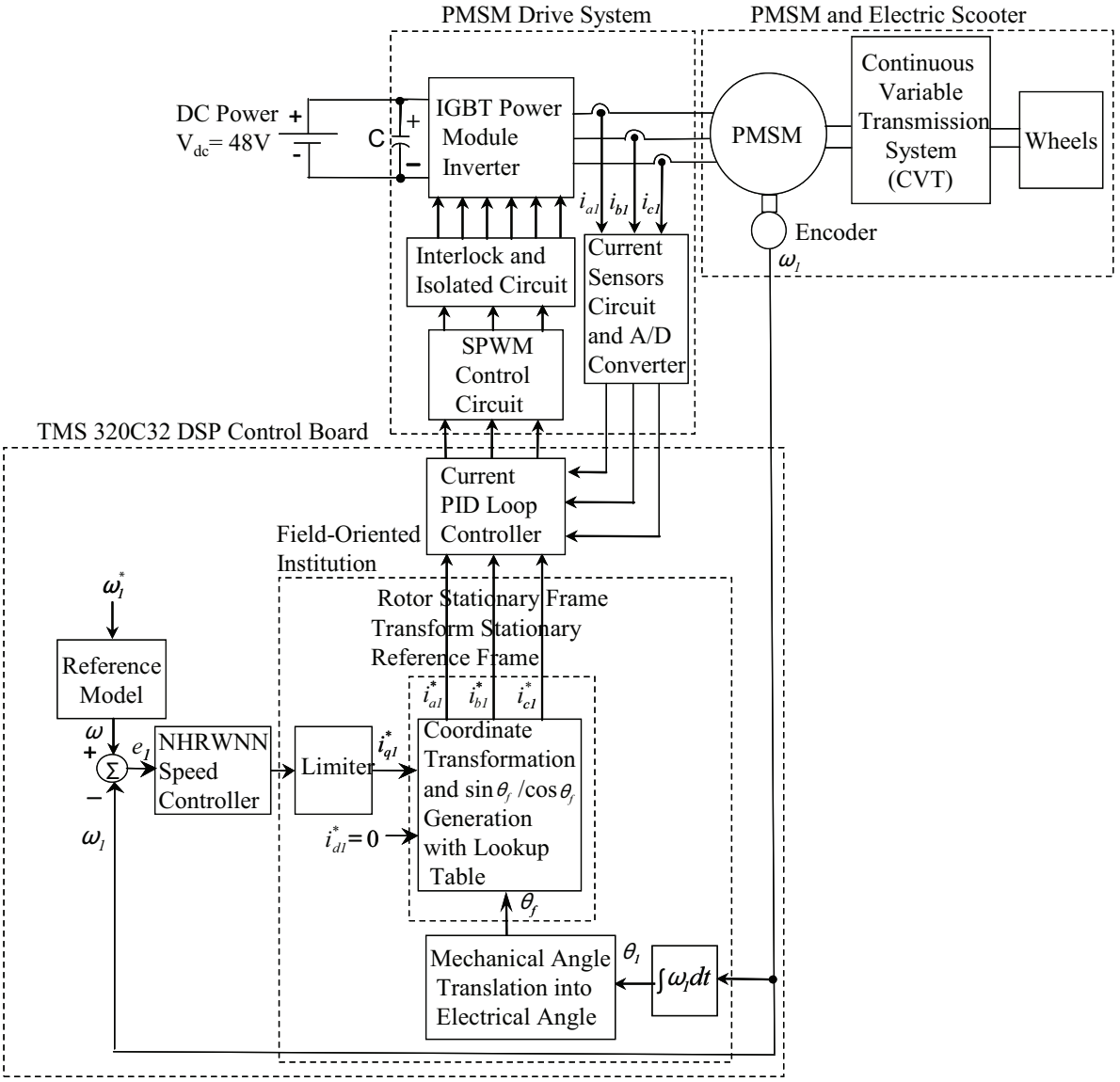

Figure 1. Block diagram of a PMSM drive electric scooter system.

1.2. The NHRWNN control system design

For convenient NHRWNN control system design, the dynamic equation of the PMSM drive electric scooter system from Eq. (2) can be rewritten as:

$$\dot{\omega}_1 = -B_1\omega_1/J_1 + K_e i_{q1}^*/J_1 - T_{L1}/J_1 = A_H\omega_1 + B_H U_H + C_H T_{L1}. \tag{7}$$

Here, ω_1 is the rotor speed of the PMSM, i_{q1}^* is the command current of the stator of the PMSM, and $A_H = -B_1/J_1$, $B_H = K_e/J_1$, and $C_H = -1/J_1$ are known constants. When uncertainties including variation of system parameters and external force disturbance occur, the parameters are assumed to be bounded. That is, $|A_H\omega_r| \le L_1^U(\omega_r)$, $|C_H T_{L1}| \le L_2^U$, and $L_3 \le B_H$, where $L_1^U(\omega_r)$ is a known continuous function and L_2^U and

L_3 are known constants. The tracking error can then be defined as follows:

$$e_1 = \omega - \omega_1, \tag{8}$$

where ω represents the desired rotor speed, and e_1 is the tracking error between the desired rotor speed and rotor speed. If all parameters of the PMSM drive system including external load disturbance are well known, the ideal control law can be designed as [31–33]:

$$U_H^* = \left[-A_H\omega_1 - C_H T_{L1} + \dot{\omega} + k_a e_1\right]/B_H, \tag{9}$$

in which k_a is positive constant. Replacing Eq. (9) for Eq. (7), the error dynamic equation can be obtained:

$$\dot{e}_1 + k_a e_1 = 0. \tag{10}$$

The system state can track the desired trajectory gradually if $e_1(t) \to 0$ as $t \to \infty$ in Eq. (10). However, the NHRWNN control system is proposed to control the PMSM to drive the electric scooter due to uncertainties effect. The configuration of the proposed NHRWNN control system is described in Figure 2. The NHRWNN control system is composed of a supervised control, a RWNN controller, and a compensated control system. The control law is designed as follows [28,32,33]:

$$U_H = U_{1S} + U_{2R} + U_{3C}. \tag{11}$$

The designed idea of the proposed supervised control U_{1S} is capable of stabilizing around a predetermined bound area in the states of the controlled system. Since supervised control caused the overdone and chattering control effort, the RWNN control and compensated control are proposed to reduce and smooth the control effort when the system states are inside the predetermined bound area. The RWNN control U_{2R} is the major tracking controller. It is used to imitate an ideal control law. The compensated control U_{3C} is designed to compensate the difference between the ideal control law and the RWNN control. When the RWNN approximation properties cannot be ensured, the supervised control law is able to act in this case.

For the condition of divergence of states, the design of a NHRWNN control system is essential to stretch the divergent states back to the predestinated bound area. The NHRWNN control system can uniformly approximate the ideal control law inside the bound area. The stability of the NHRWNN control system can then be warranted. An error dynamic equation from Eq. (7) to Eq. (11) can be acquired as:

$$\dot{e}_1 = -k_a e_1 + [U_H^* - U_{1S} - U_{2R} - U_{3C}]B_H. \tag{12}$$

The Lyapunov function is then chosen as:

$$V_1 = e_1^2/2. \tag{13}$$

Differentiating Eq. (13) with respect to t and substituting Eq. (12) into Eq. (13), we have the following.

$$\dot{V}_1 = e_1\dot{e}_1 = e_1[-k_a e_1 + [U_H^* - U_{2R} - U_{2C} - U_{1S}]B_H] \le -k_a e_1^2 + |e_1 B_H| \cdot [|U_H^*| + |U_{2R} + U_{3C}|] - e_1 B_H U_{1S} \tag{14}$$

To suffice for $\dot{V}_1 \le 0$, the supervised control U_{1S} is designed as follows [33]:

$$U_{1S} = I_{1S} sgn\left(e_1 B_H\right)\left[|U_{2R} + U_{3C}| + \left(L_1^U(\omega_1) + L_2^U + |\omega| + |k_a e_1|\right)/B_H\right], \tag{15}$$

in which $sgn(\cdot)$ is a sign function, and the operating indicator can be adopted as:

$$I_{1S} = \begin{cases} I_{1S} = 1, & \text{if } V_1 \geq \bar{V}_1 \\ I_{1S} = 0, & \text{if } V_1 < \bar{V}_1 \end{cases}, \tag{16}$$

where $\bar{V}_1$ is a positive constant. Selecting $I_{1S} = 1$ and using Eq. (15), Eq. (14) can then be obtained as follows.

$$\begin{aligned} \dot{V}_1 &\leq -k_a e_1^2 + |e_1 B_H| \left[|U_H^*| + |U_{2R} + U_{3C}| \right] - e_1 B_H U_{1S} \\ &\leq -k_a e_1^2 + |e_1 B_P| \left[|A_H \omega_1| + |C_H T_L| + |\dot{\omega}| + |k_a e_1| \right] / B_H + \left[|U_{2R} + U_{3C}| \right] - \left[|U_{2R} + U_{3C}| \right] \\ &- |e_1 B_H| \left[L_1^U(\omega_1) + L_2^U + |\dot{\omega}| + |k_a e_1| \right] / B_H \\ &\leq -k_a e_1^2 \leq 0 \end{aligned} \tag{17}$$

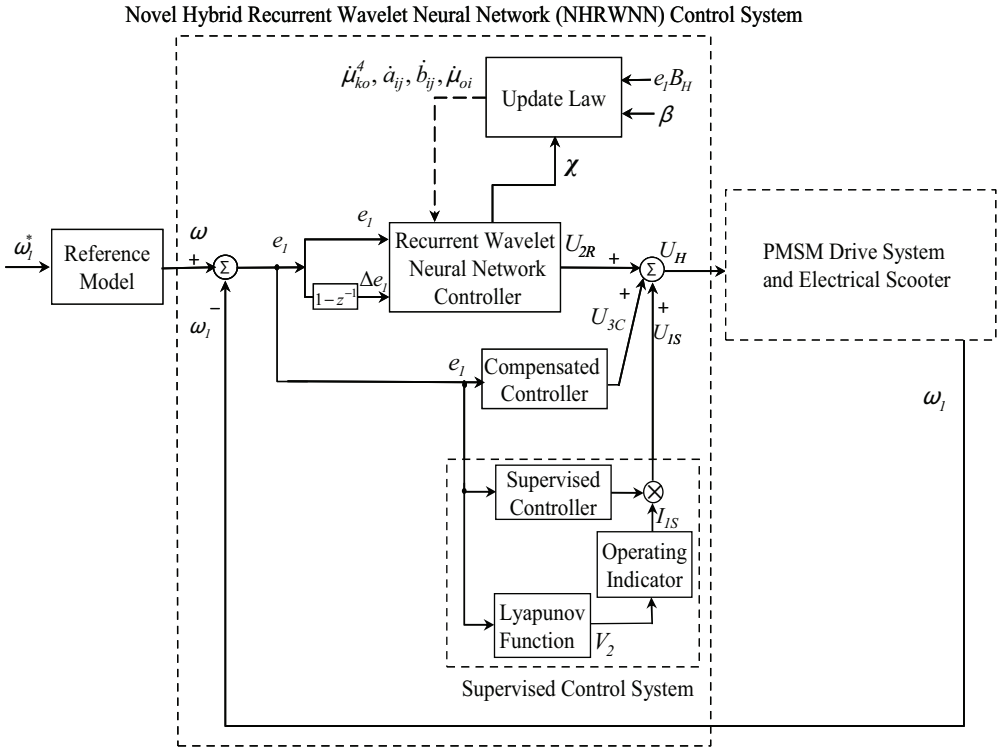

Figure 2. Block diagram of NHRWNN control system.

The supervised control system is capable of causing the tracking error to be 0 according to Eq. (17) without using RWNN control and the compensated control system. Due to the selection of the bound values, e.g., $L_1^U(\omega_1), L_2^U$, L_3, and sign function, the supervised control can produce an overdone and chattering control effort. Therefore, the RWNN control and compensated control can be devised to conquer the mentioned blemish. The RWNN control is raised to imitate the ideal control U_H^*. The compensated control is then poised to compensate the difference between U_H^* and the RWNN control. The architecture of the proposed 4-layer RWNN is depicted in Figure 3. It is composed of an input, a mother wavelet, a wavelet, and an output layer. The activation functions and signal actions of nodes in each layer of the RWNN can be described as follows.

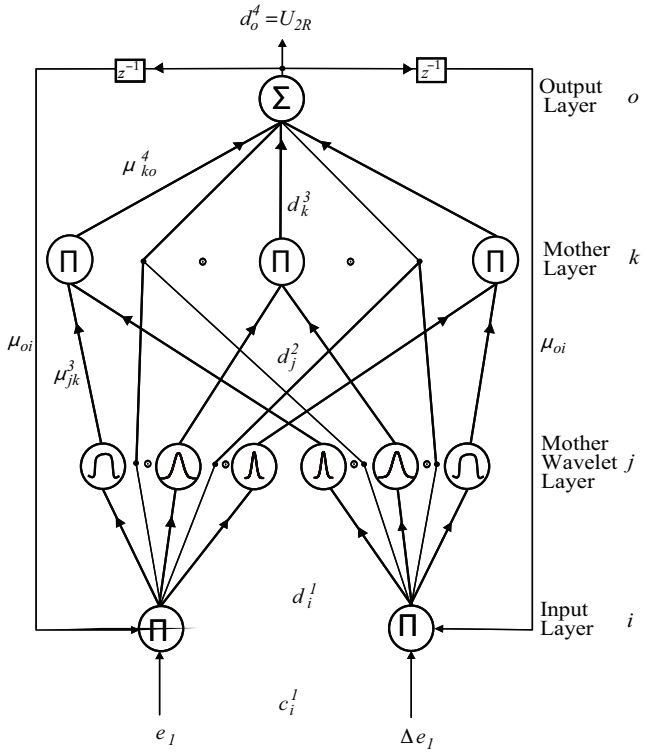

Figure 3. Structure of the 4-layer RWNN.

Layer 1: Input layer

Each node $i$in this layer is indicated by using $\prod$ which multiply by each other between each other for input signals. The outputs signals are then the results of the product. The input and the output for each node i in this layer are expressed as:

$$nod_i^1(N) = \prod_o c_i^1(N)\mu_{oi}d_o^4(N-1), d_i^1(N) = g_i^1(nod_i^1(N)) = nod_i^1(N), i = 1, 2. \tag{18}$$

Here, $c_1^1 = \omega - \omega_1 = e_1$ is the tracking error between the desired speed ω and the rotor angular speed ω_1, and $c_2^1 = e_1(1 - z^{-1}) = \Delta e_1$ is the tracking error change. N denotes the number of iterations and d_o^4 is the output value from the output layer of the RWNN.

Layer 2: Mother wavelet layer

A family of wavelets is constructed by translations and dilations performed on the mother wavelet. In the mother wavelet layer, each node performs a wavelet $\varphi(x)$that is derived from its mother wavelet. There are many kinds of wavelets that can be used in a WNN. In this paper, the first derivative of the Gaussian wavelet function $\theta(x) = -x\exp(-x^2/2)$ is adopted as a mother wavelet [30]. The input and the output for each jth node in this layer are expressed as:

$$nod_j^2(N) = \frac{c_i^2 - a_{ij}}{b_{ij}}, d_j^2(N) = g_j^2(nod_j^2(N)) = \varphi(nod_j^2(N)), j = 1, \cdots, n \tag{19}$$

Here, a_{ij} and b_{ij} are the translations and dilations in the jth term of the ith input $c_i^2$to the node of the mother wavelet layer, and $n$is the total number of the wavelets with respect to the input nodes.

Layer 3: Mother layer

Each node k in this layer is indicated by using $\prod$, which multiply by each other between each other for input signals. The outputs signals are then the results of the product. The inputs and the outputs for each kth node in this layer are expressed as:

$$nod_k^3(N) = \prod_j \mu_{jk}^3 c_j^3(N), d_k^3(N) = g_k^3(nod_k^3(N)) = nod_k^3(N), \quad k = 1, 2, \cdots, l_1, \tag{20}$$

where c_j^3 represents the jth input to the node of layer 3, and μ_{jk}^3 are the weights between the mother wavelet layer and the wavelet layer. They are assumed to be unity; $l_1 = (n/i)$ is the number of wavelets if each input node has the same mother wavelet nodes.

Layer 4: Output layer

The single oth node in this layer is labeled with $\sum$. It computes the overall output as the summation of all input signals. The net input and the net output for the oth node in this layer are expressed as:

$$nod_o^4(N) = \sum_k \mu_{ko}^4 c_k^4(N), d_o^4(N) = g_o^4(nod_o^4(N)) = nod_o^4(N), o = 1. \tag{21}$$

The connecting weight μ_{ko}^4 is the output action strength of the oth output associated with the kth node; c_k^4 represents the kth input to the node of layer 4. The output value of the RWNN can be represented as $d_o^4 = U_{2R}$. The output value of the RWNN, U_{2R}, can then be denoted as:

$$U_{2R} = (\psi)^T \chi. \tag{22}$$

Here, $\psi = \left[\mu_{11}^4 \mu_{21}^4 \cdots \mu_{l1}^4\right]^T$ is the adjustable weight parameter vector between the mother layer and the output layer of the RWNN. Furthermore, $\chi = \left[c_1^4 c_2^4 \cdots c_l^4\right]^T$ is the input vector in the output layer of the RWNN, in which c_k^4 is determined by the selected mother wavelet function and $0 \le c_k^4 \le 1$.

In order to evolve the compensated control U_{3C}, a minimum approximation error σ is defined as:

$$\sigma = U_H^* - U_{2R}^* = U_H^* - (\psi^*)^T \chi. \tag{23}$$

Here, ψ^* is an optimal weight vector to reach a minimum approximation error. It is assumed that the absolute value of σ is less than a small positive constant α, i.e. $|\sigma| < \alpha$. The error dynamic equation can then be rewritten as follows.

$$\begin{aligned} \dot{e}_1 &= -k_a e_1 + B_H \left\{[U_H^* - U_{2R}] - U_{3C} - U_{1S}\right\} \\ &= -k_a e_1 + B_H \left\{[U_H^* - U_{2R}^* + U_{2R}^* - U_{2R}] - U_{3C} - U_{1S}\right\} \\ &= -k_a e_1 + B_H \left\{\left[U_H^* - U_{2R}^* + (\psi^*)^T \chi - (\psi)^T \chi\right] - U_{3C} - U_{1S}\right\} \\ &= -k_a e_1 + B_H \left\{\sigma + (\psi^* - \psi)^T \chi - U_{3C} - U_{1S}\right\} \end{aligned} \tag{24}$$

The Lyapunov function is then selected as:

$$V_2 = e_1^2/2 + (\psi^* - \psi)^T (\psi^* - \psi)/(2\beta). \tag{25}$$

Differentiating the Lyapunov function with respect to t and using Eq. (24), Eq. (25) can be rewritten as:

$$\begin{aligned} \dot{V}_2 &= e_1 \dot{e}_1 - (\psi^* - \psi)^T \dot{\psi}/\beta \\ &= -k_a e_1^2 + e_1 B_H \left\{\sigma - U_{3C} - U_{1S}\right\} + e_1 B_H \left(\psi^* - \psi\right)^T \chi - (\psi^* - \psi)^T \dot{\psi}/\beta \end{aligned} . \tag{26}$$

The adaptive law $\dot{\psi}$ and the compensated controller U_{3C} to satisfy $\dot{V}_2 \leq 0$ can be designed as:

$$\dot{\psi} = \beta e_1 B_H, \tag{27}$$

$$U_{3C} = \alpha sgn(e_1 B_H), \tag{28}$$

in which $\beta > 0$ is denoted as an adaptation gain. From Eq. (15) and Eq. (27), Eq. (26) can be represented as:

$$\dot{V}_2 = -k_a e_1^2 + e_1 B_H \{\sigma - U_{3C} - U_{1S}\} \leq -k_a e_1^2 + e_1 B_H \{\sigma - U_{3C}\}. \tag{29}$$

From Eq. (28), Eq. (29) can be obtained as:

$$\dot{V}_2 \leq -k_a e_1^2 + e_1 B_H \{\sigma - U_{3C}\} \leq -k_a e_1^2 + |e_1 B_H| \{|\sigma| - \alpha\} \leq -k_a e_1^2 \leq 0. \tag{30}$$

From Eq. (30), $\dot{V}_2$ is negative semidefinite, i.e. $V_2(t) \leq V_2(0)$. This implies that e_1 and $(\psi^* - \psi)$ are bounded. For proof of the NHRWNN control system being gradually stable, let the function be defined as:

$$\Omega(t) = -\dot{V}_2(t) = k_a e_1^2. \tag{31}$$

Integrating Eq. (31) with respect to t gives:

$$\int_0^t \Omega(t) d\tau = \int_0^t -\dot{V}_2(t) dt = V_2(0) - V_2(t). \tag{32}$$

Due to $V_2(0)$ being bounded and $V_2(t)$ being nonincreasing and bounded, then:

$$\lim_{t \to \infty} \int_0^t \Omega(t) d\tau < \infty. \tag{33}$$

Differentiating Eq. (31) with respect to t gives:

$$\dot{\Omega}(t) = 2k_a e_1 \dot{e}_1. \tag{34}$$

Due to all the variables on the right-hand side of Eq. (24) being bounded, it is implied that $\dot{e}_1$ is also bounded. Therefore, $\Omega(t)$ is a uniformly continuous function [34,35]. It is denoted that $\lim_{t \to \infty} \Omega(t) = 0$ by using Barbalat's lemma [34,35]. Therefore, $e(t) \to 0$ as $t \to \infty$. From the above proof, the NHRWNN control system is gradually stable. Moreover, the tracking error e_1 of the system will converge to 0 according to $e_1(t) = 0$.

According to the Lyapunov stability theorem and the gradient descent method, an on-line parameter training methodology of the RWNN can be derived and trained effectively. The parameters of adaptation laws $\dot{\psi}(\mu_{ko}^4, a_{ij}, b_{ij}, \mu_{oi})$ can then be computed by the gradient descent method and the backpropagation algorithm as follows.

$$\dot{\mu}_{ko}^4 = \beta e_1 B_H \chi \underline{\Delta} - \beta \frac{\partial V_2}{\partial U_{2R}} \frac{\partial U_{2R}}{\partial d_o^4} \frac{\partial d_o^4}{\partial nod_o^4} \frac{\partial nod_o^4}{\partial \mu_{ko}^4} = -\beta \frac{\partial V_2}{\partial U_{2R}} c_k^4 \tag{35}$$

The above Jacobian term of control system can be rewritten as $\partial V_2 / \partial U_{2R} = -e_1 B_H$. The first error term can then be counted as:

$$\upsilon_k^3 \underline{\Delta} - \frac{\partial V_2}{\partial U_{2R}} \frac{\partial U_{2R}}{\partial d_o^4} \frac{\partial y_o^4}{\partial nod_o^4} \frac{\partial nod_o^4}{\partial d_k^3} \frac{\partial d_k^3}{\partial nod_k^3} = e_1 B_H \mu_{ko}^4. \tag{36}$$

The second error term of mother wavelet function can be computed as follows.

$$\upsilon_j^2 \triangleq -\frac{\partial V_2}{\partial U_{2R}}\frac{\partial U_{2R}}{\partial d_o^4}\frac{\partial d_o^4}{\partial nod_o^4}\frac{\partial nod_o^4}{\partial d_k^3}\frac{\partial d_k^3}{\partial nod_k^3}\frac{\partial nod_k^3}{\partial d_j^2}\frac{\partial d_j^2}{\partial nod_j^2} = \sum_k \upsilon_k^3 d_k^3(N) \tag{37}$$

The translation a_{ij} and dilation b_{ij} of the Gaussian wavelet function can be renewed by using the gradient descent method as:

$$\dot{a}_{ij} = -\frac{\partial V_2}{\partial nod_j^2}\frac{\partial nod_j^2}{\partial a_{ij}} = \upsilon_j^2\frac{(c_i^2 - a_{ij})}{b_{ij}} \tag{38}$$

$$\dot{a}_{ij} = -\frac{\partial V_2}{\partial nod_j^2}\frac{\partial nod_j^2}{\partial a_{ij}} = \upsilon_j^2\frac{(c_i^2 - a_{ij})}{b_{ij}} \tag{39}$$

The recurrent weight μ_{oi} can be renewed as:

$$\dot{\mu}_{oi} = -\frac{\partial V_2}{\partial nod_j^2}\frac{\partial nod_j^2}{\partial d_i^1}\frac{\partial d_i^1}{\partial nod_i^1}\frac{\partial nod_i^1}{\partial \mu_{oi}} = \sum_j \upsilon_j^2\frac{(c_i^2(N) - a_{ij})}{b_{ij}}c_i^1(N)d_o^4(N-1). \tag{40}$$

2. Experimental results

The whole system of the DSP-based control system for a PMSM drive electric scooter system is shown in Figure 1. A photo of the experimental set-up is shown in Figure 4. The control algorithm was executed by a TMS320C32 DSP control system that includes multiple channels of D/A, 8 channels of programmable PWM, and encoder interface circuits. The IGBT power modules' voltage source inverter is executed by current-controlled SPWM with a switching frequency of 15 kHz. The current PID loop controller is the current loop tracking controller. The control gains $K_{P,}K_I, K_D$ of the current PID loop controller are $K_P = 15, K_I = 2, K_D = 0.5$ to attain good current dynamic response by using a trial-and-error method. The specifications of the used PMSM are 3 phases, 48 V, 750 W, 16.5 A, and 3600 rpm. The parameters of the PMSM are as follows: $R_1 = 2.5\Omega$, $L_{d1} = L_{q1} = 6.53mH$, $K_e = 0.86Nm/A$, $\bar{J}_1 = 2.15 \times 10^{-3}Nms$, $\bar{B}_1 = 6.18 \times 10^{-3}Nms/rad$, based on use of open circuit test, short test, rotor block test, and loading test.

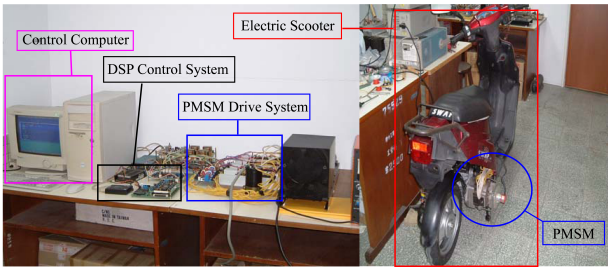

Figure 4. Photo of the experimental set-up.

The NHRWNN control performance is compared with 2 baseline controllers: the PI and the PID controllers. The PI, PID, and NHRWNN methods are tested through 2 cases. To show the control performance of the proposed NHRWNN control system, 2 cases are provided in the experimentation. Due to inherent uncertainty in the electric scooter and output current limitation of battery power capacity, a PMSM can only operate at 251.2 rad/s (2400 rpm) due to high speed perturbation. Two cases are provided in the experimentation

here, the first being the 125.6 rad/s (1200 rpm) caseand the second being the 251.2 rad/s (2400 rpm) case. Since the electric scooter is a nonlinear time-varying system, the gains of the PI and PID controllers for the speed tracking are obtained by trial-and-error in order to achieve good transient and steady-state control performance in the 125.6 rad/s (1200 rpm) case. The control gains of the PI controller are $K_P = 12.5, K_I = 1.2$ in the 125.6 rad/s (1200 rpm) case for the speed tracking. The experimental results of the PI controller for a PMSM-driven electric scooter for the 125.6 rad/s (1200 rpm) case are shown in Figure 5, where tracking responses of the command rotor angular speed ω_1^*, the desired command rotor angular speed ω, and the measured rotor angular speed ω_1 are shown in Figure 5a; tracking responses of the command rotor position θ_1^* and the measured rotor position θ_1 are shown in Figure 5b; tracking responses of the command current i_{a1}^* and the measured current i_{a1} in phase *a1* are shown in Figure 5c; and tracking responses of the command current i_{b1}^* and measured current i_{b1} in phase *b1* are shown in Figure 5d. The experimental results of the PI controller for a PMSM-driven electric scooter in the 251.2 rad/s (2400 rpm) case are shown in Figure 6, where tracking responses of the command rotor angular speed ω_1^*, the desired command rotor angular speed ω, and the measured rotor angular speed ω_1 are shown in Figure 6a; tracking responses of the command rotor position θ_1^* and the measured rotor position θ_1 are shown in Figure 6b; tracking responses of the command current i_{a1}^* and the measured current i_{a1} in phase *a1* are shown in Figure 6c; and tracking responses of the command current i_{b1}^* and measured current i_{b1} in phase *b1* are shown in Figure 6d. The control gains of the PID controller are $K_P = 13.2, K_I = 2.1, K_D = 1.2$ in the 125.6 rad/s (1200 rpm) case for the speed tracking. The experimental results of the PID controller for a PMSM-driven electric scooter for the 125.6 rad/s (1200 rpm) case are shown in Figure 7, where tracking responses of the command rotor angular speed ω_1^*, the desired command rotor angular speed ω, and the measured rotor angular speed ω_1 are shown in Figure 7a; tracking responses of the command rotor position θ_1^* and the measured rotor position θ_1 are shown in Figure 7b; tracking responses of the command current i_{a1}^* and the measured current i_{a1} in phase *a1* are shown in Figure 7c; and tracking responses of the command current i_{b1}^* and measured current i_{b1} in phase *b1* are shown in Figure 7d. The experimental results of the PID controller for a PMSM-driven electric scooter in the 251.2 rad/s (2400 rpm) case are shown in Figure 8, where tracking responses of the command rotor angular speed ω_1^*, the desired command rotor angular speed ω, and the measured rotor angular speed ω_1 are shown in Figure 8a; tracking responses of the command rotor position θ_1^* and the measured rotor position θ_1 are shown in Figure 8b; tracking responses of the command current i_{a1}^* and the measured current i_{a1} in phase *a1* are shown in Figure 8c; and tracking responses of the command current i_{b1}^* and measured current i_{b1} in phase *b1* are shown in Figure 8d. The degenerate tracking responses in Figures 6a and 8a result from the occurrence of parameter variation and external load disturbance. From the experimental results, sluggish speed tracking is obtained for the PI- and PID-controlled PMSM-driven electric scooter due to the weak robustness of the linear controller.

The control gains of the proposed NHRWNN control system are $\alpha = 0.1$, $\beta = 0.5$, $\sigma = 0.05$. All the gains in the NHRWNN control system are chosen to achieve the best transient control performance in experimentation considering the requirement of stability. For testing performance, the RWNN is adopted in the 4-layer structure with different nodes in the input layer, the mother wavelet layer, the wavelet layer, and the output layer. The initialization of the wavelet network parameters in [36] is adopted to initialize the parameters of the wavelets. The effect due to inaccurate selection of the initialized parameters can be retrieved by the on-line parameter training methodology. The parameter adjustment process remains continually active for the duration of the experimentation. For testing performance for the 4-layer RWNN with different nodes, 2 different nodes are provided in experimentation. The first kind of RWNN in the NHRWNN control system has 2 nodes,

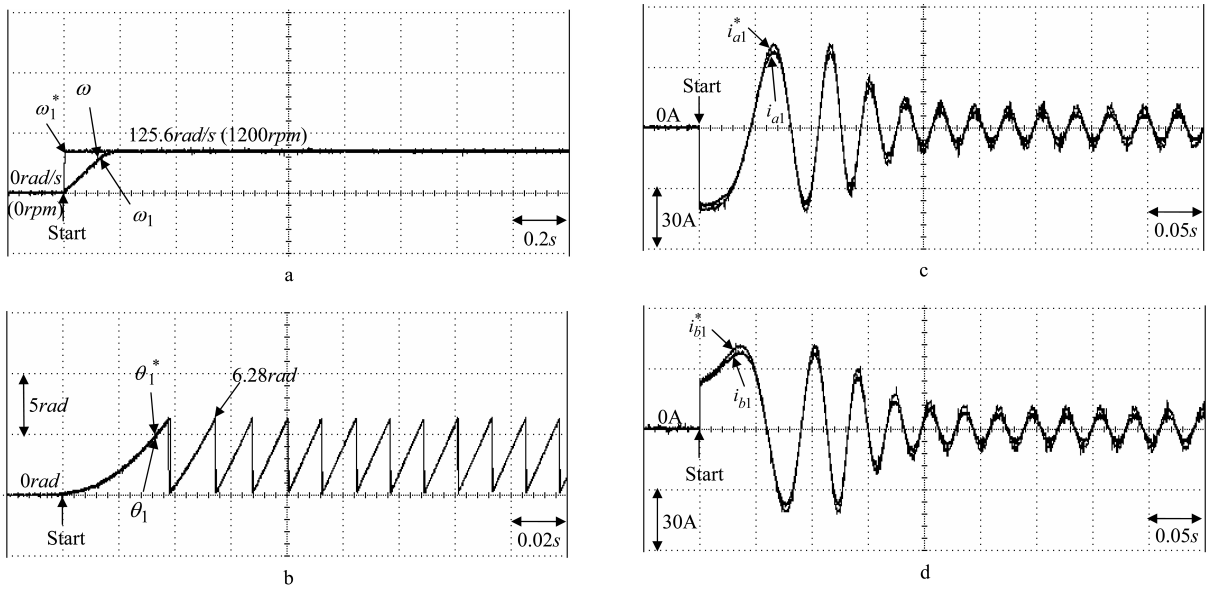

Figure 5. Experimental results of PI controller for a PMSM drive electric scooter at 125.6 rad/s (1200 rpm): a) command rotor angular speed ω_1^*, desired command rotor angular speed ω, and measure rotor angular speed ω_1; b) command rotor position θ_1^* and measured rotor position θ_1; c) command current i_{a1}^* and measured current i_{a1} in phase *a1*; d) command current i_{b1}^* and measured current i_{b1} in phase *b1*.

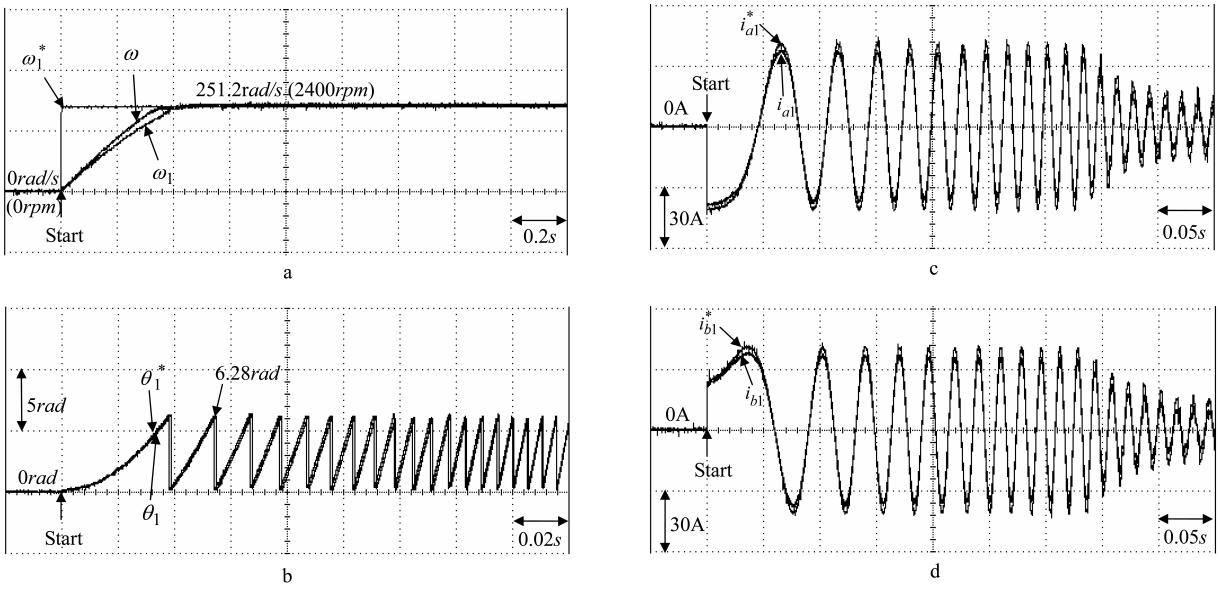

Figure 6. Experimental results of PI controller for a PMSM drive electric scooter at 251.2 rad/s (2400 rpm): a) command rotor angular speed ω_1^*, desired command rotor angular speed ω, and measured rotor angular speed ω_1; b) command rotor position θ_1^* and measured rotor position θ_1; c) command current i_{a1}^* and measured current i_{a1} in phase *a1*; d) command current i_{b1}^* and measured current i_{b1} in phase *b1*.

14 nodes, 7 nodes, and 1 node in the input layer, the mother wavelet layer, the wavelet layer, and the output layer, respectively. The second kind of RWNN in the NHRWNN control system has 2 nodes, 10 nodes, 5 nodes, and 1 node in the input layer, the mother wavelet layer, the wavelet layer, and the output layer, respectively. The experimental results of the first kind of RWNN in the NHRWNN control system for a PMSM-driven electric

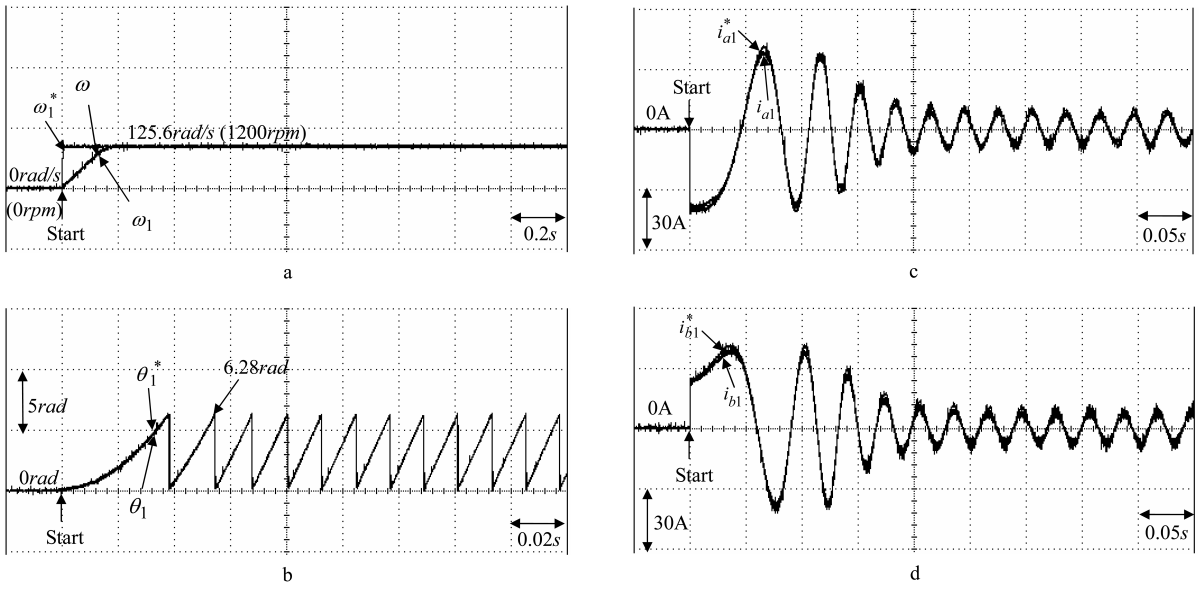

Figure 7. Experimental results of PID controller for a PMSM drive electric scooter at 125.6 rad/s (1200 rpm): a) command rotor angular speed ω_1^*, desired command rotor angular speed ω, and measure rotor angular speed ω_1; b) command rotor position θ_1^* and measured rotor position θ_1; c) command current i_{a1}^* and measured current i_{a1} in phase *a1*; d) command current i_{b1}^* and measured current i_{b1} in phase *b1*.

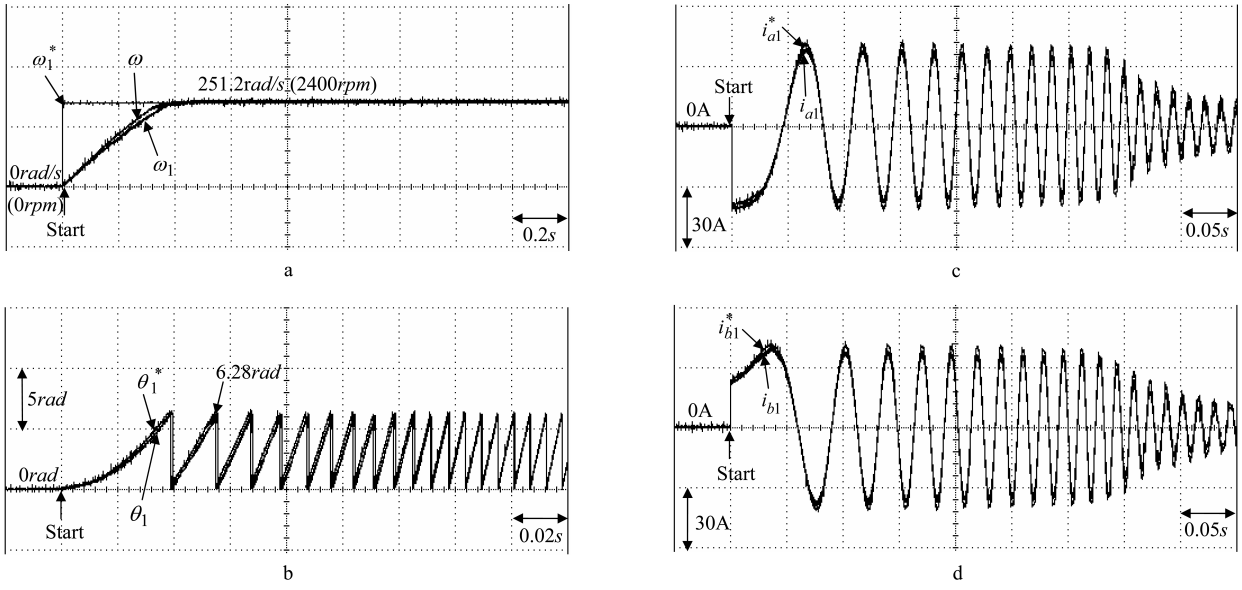

Figure 8. Experimental results of PID controller for a PMSM drive electric scooter at 251.2 rad/s (2400 rpm): a) command rotor angular speed ω_1^*, desired command rotor angular speed ω, and measured rotor angular speed ω_1; b) command rotor position θ_1^* and measured rotor position θ_1; c) command current i_{a1}^* and measured current i_{a1} in phase *a1*; d) command current i_{b1}^* and measured current i_{b1} in phase *b1*.

scooter in the 125.6 rad/s (1200 rpm) case are shown in Figure 9, where tracking responses of the command rotor angular speed ω_1^*, the desired command rotor angular speed ω, and the measured rotor angular speed ω_1 are shown in Figure 9a; tracking responses of the command rotor position θ_1^* and the measured rotor position θ_1 are shown in Figure 9b; tracking responses of the command current i_{a1}^* and the measured current i_{a1} in

phase *a1* are shown in Figure 9c; and tracking responses of the command current i_{b1}^* and measured current i_{b1} in phase *b1* are shown in Figure 9d. The experimental results of the first kind of RWNN in the NHRWNN control system for a PMSM-driven electric scooter in the 251.2 rad/s (2400 rpm) case are shown in Figure 10, where tracking responses of the command rotor angular speed ω_1^*, the desired command rotor angular speed ω, and the measured rotor angular speed ω_1 are shown in Figure 10a; tracking responses of the command rotor position θ_1^* and the measured rotor position θ_1 are shown in Figure 10b; tracking responses of the command current i_{a1}^* and the measured current i_{a1} in phase *a1* are shown in Figure 10c; and tracking responses of the command current i_{b1}^* and measured current i_{b1} in phase *b1* are shown in Figure 10d. The experimental results of the second kind of RWNN in the NHRWNN control system for a PMSM-driven electric scooter in the 125.6 rad/s (1200 rpm) case are shown in Figure 11, where tracking responses of the command rotor angular speed ω_1^*, the desired command rotor angular speed ω, and the measured rotor angular speed ω_1 are shown in Figure 11a; tracking responses of the command rotor position θ_1^* and the measured rotor position θ_1 are shown in Figure 11b; tracking responses of the command current i_{a1}^* and the measured current i_{a1} in phase *a1* are shown in Figure 11c; and tracking responses of the command current i_{b1}^* and measured current i_{b1} in phase *b1* are shown in Figure 11d. The experimental results of the second kind of RWNN in the NHRWNN control system for a PMSM-driven electric scooter in the 251.2 rad/s (2400 rpm) case are shown in Figure 12, where tracking responses of the command rotor angular speed ω_1^*, the desired command rotor angular speed ω, and the measured rotor angular speed ω_1 are shown in Figure 12a; tracking responses of the command rotor position θ_1^* and the measured rotor position θ_1 are shown in Figure 12b; tracking responses of the command current i_{a1}^* and the measured current i_{a1} in phase *a1* are shown in Figure 12c; and tracking responses of the command current i_{b1}^* and measured current i_{b1} in phase *b1* are shown in Figure 12d. However, owing to the on-line adaptive mechanism of the RWNN and the compensated controller, accurate tracking control performance of the PMSM can be obtained. These results show that the NHRWNN control system has better performances

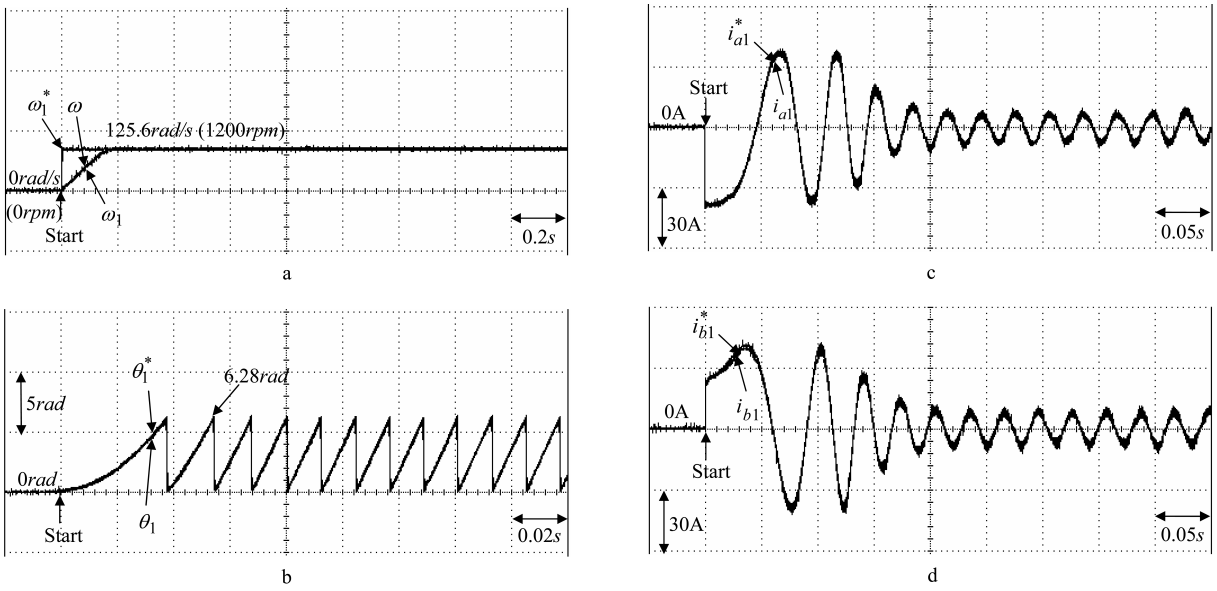

Figure 9. Experimental results of the first kind of RWNN in the NHRWNN control system for a PMSM drive electric scooter at 125.6 rad/s (1200 rpm): a) command rotor angular speed ω_1^*, desired command rotor angular speed ω, and measured rotor angular speed ω_1; b) command rotor position θ_1^* and measured rotor position θ_1; c) command current i_{a1}^* and measured current i_{a1} in phase *a1*; d) command current i_{b1}^* and measured current i_{b1} in phase *b1*.

than the PI and PID controllers for speed perturbation for a PMSM-driven electric scooter. Additionally, the small chattering phenomena that existed in phase *a1* and in phase *b1*, as shown in Figures 10c, 10d, 12c, and 12d, are induced by on-line adjustment of the RWNN to cope with the high-frequency unmodeled dynamics of the controlled plant.

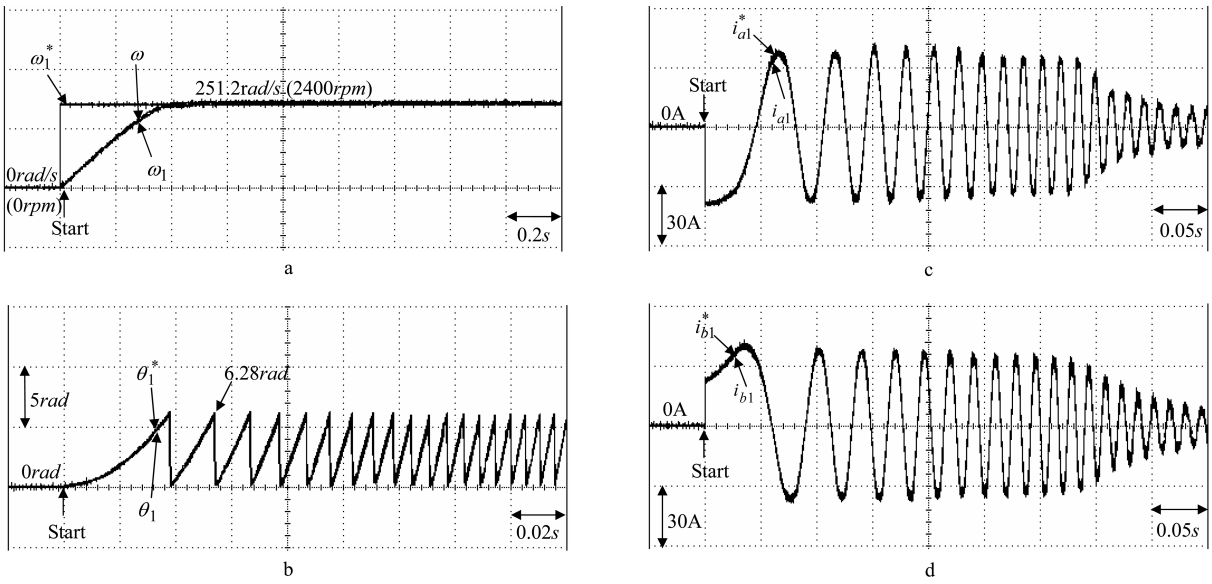

Figure 10. Experimental results of the first kind of RWNN in the NHRWNN control system for a PMSM drive electric scooter at 251.2 rad/s (2400 rpm): a) command rotor angular speed ω_1^*, desired command rotor angular speed ω, and measured rotor angular speed ω_1; b) command rotor position θ_1^* and measured rotor position θ_1; c) command current i_{a1}^* and measured current i_{a1} in phase *a1*; d) command current i_{b1}^* and measured current i_{b1} in phase *b1*.

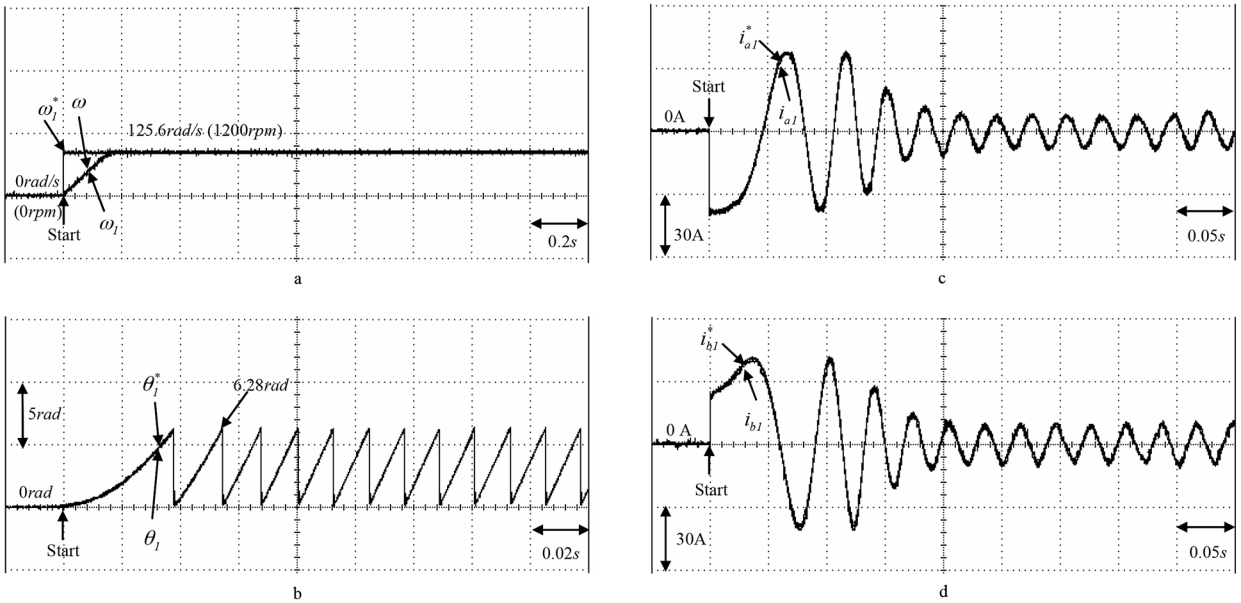

Figure 11. Experimental results of the second kind of RWNN in the NHRWNN control system for a PMSM drive electric scooter at 125.6 rad/s (1200 rpm): a) command rotor angular speed ω_1^*, desired command rotor angular speed ω, and measured rotor angular speed ω_1; b) command rotor position θ_1^* and measured rotor position θ_1; c) command current i_{a1}^* and measured current i_{a1} in phase *a1*; d) command current i_{b1}^* and measured current i_{b1} in phase *b1*.

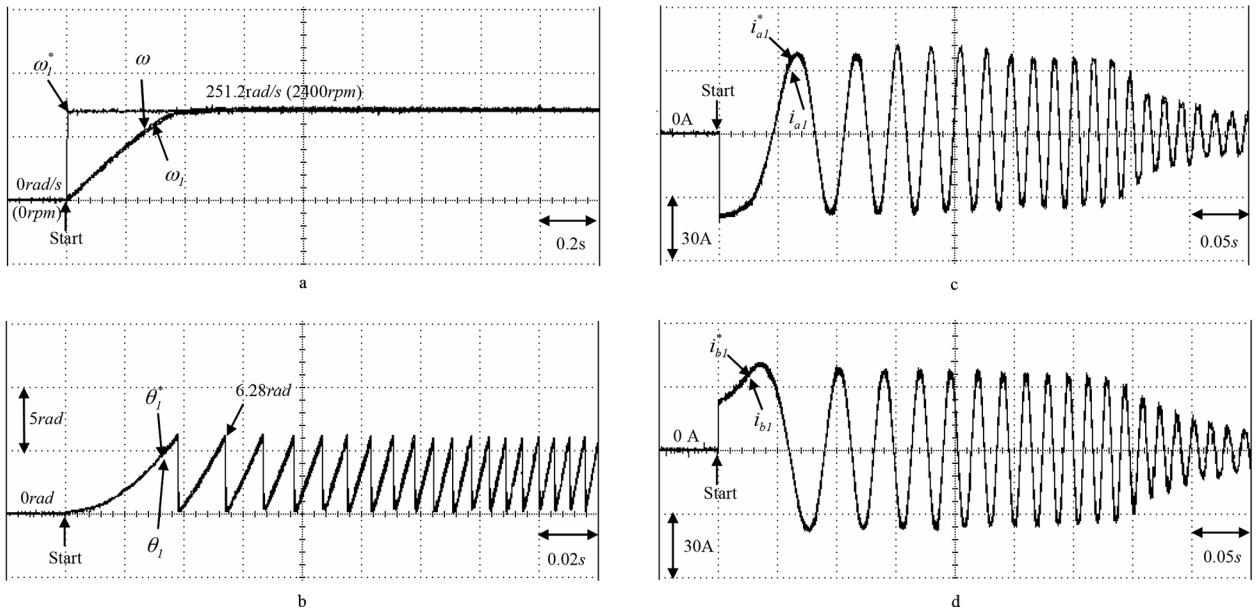

Figure 12. Experimental results of the second kind of RWNN in the NHRWNN control system for a PMSM drive electric scooter at 251.2 rad/s (2400 rpm): a) command rotor angular speed ω_1^*, desired command rotor angular speed ω, and measured rotor angular speed ω_1; b) command rotor position θ_1^* and measured rotor position θ_1; c) command current i_{a1}^* and measured current i_{a1} in phase *a1*; d) command current i_{b1}^* and measured current i_{b1} in phase *b1*.

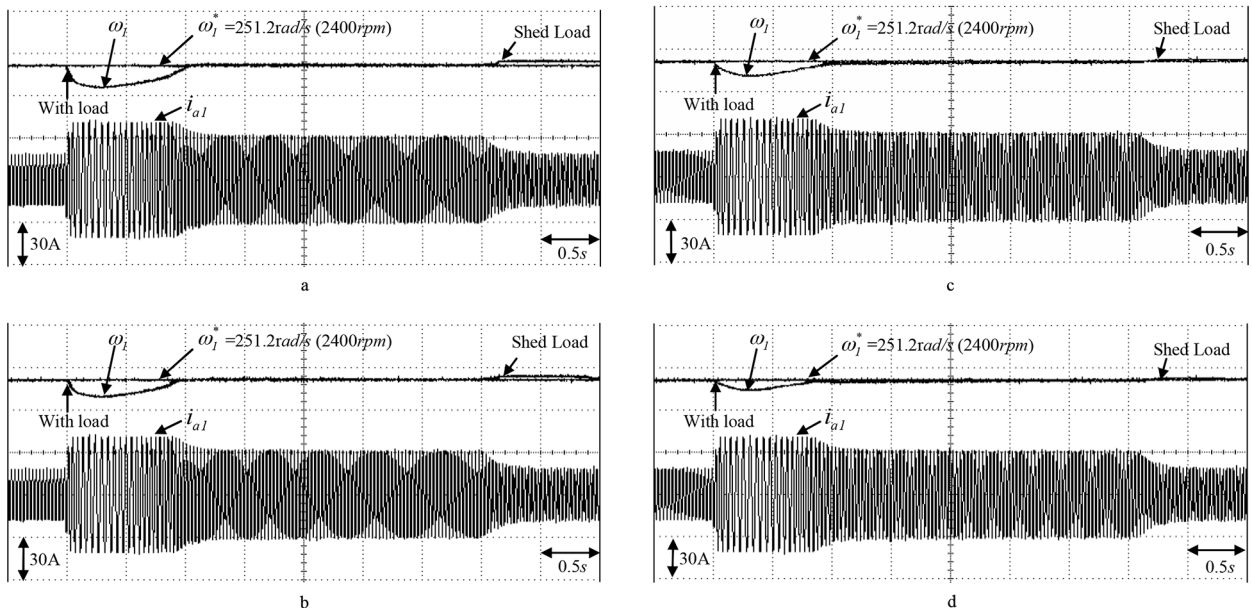

Figure 13. Experimental results due to a $T_{L1} = 2$ Nm load torque disturbance with load and shed load at 251.2 rad/s (2400 rpm): a) command rotor angular speed ω_1^*, measured rotor angular speed ω_1, and measured current i_{a1} in phase *a1* using PI controller; b) command rotor angular speed ω_1^*, measured rotor angular speed ω_1, and measured current i_{a1} in phase *a1* using PID controller; c) command rotor angular speed ω_1^*, measured rotor angular speed ω_1, and measured current i_{a1} in phase *a1* using the first kind of RWNN in the NHRWNN control system; d) command rotor angular speed ω_1^*, measured rotor angular speed ω_1, and measured current i_{a1} in phase *a1* using the second kind of RWNN in the NHRWNN control system.

The measured rotor speed responses due to step disturbance torque are given finally. The PI, PID, and NHRWNN methods are tested at $T_{L1} = 2Nm$ load torque disturbance with load and shed load. The experimental results due to a $T_{L1} = 2Nm$ load torque disturbance with load and shed load at 251.2 rad/s (2400 rpm) are shown in Figure 13, where the measured rotor speed responses and measured current in phase *a1* using the PI controller are shown in Figure 13a; the measured rotor speed responses and measured current in phase *a1* using the PID controller are shown in Figure 13b; the measured rotor speed responses and measured current in phase *a1* using the first kind of RWNN in the NHRWNN control system are shown in Figure 13c; and the measured rotor speed responses and measured current in phase *a1* using the second kind of RWNN in the NHRWNN control system are shown in Figure 13d. From the experimental results, the degenerated responses due to the variation of rotor inertia and load torque disturbance are much improved using the NHRWNN control system. From experimental results, transient response of the NHRWNN control system is better than that of the PI and PID control systems at load regulation.

3. Conclusions

A PMSM drive system controlled by a NHRWNN control system has been successfully developed to drive an electric scooter with robust control characteristics. First, the dynamic models of the PMSM drive system were derived according to the electric scooter. Since the electric scooter is a nonlinear time-varying system, sluggish speed tracking was obtained for the PI- and PID-controlled PMSM-driven electric scooter due to the weak robustness of the linear controller. Therefore, to ensure the control performance of robustness, a PMSM controlled by the NHRWNN control system was developed to drive the electric scooter. The NHRWNN control system with supervised control based on the uncertainty bounds of the controlled system was designed to stabilize the system states around a predetermined bound area. To drop the excessive chattering that resulted from the control efforts, the NHRWNN control system, which is composed of the supervised control, the RWNN, and the compensated control, was proposed to reduce and smooth the control effort when the system states are inside the predetermined bound area. Moreover, an on-line parameter training methodology was derived by using the Lyapunov stability theorem and the gradient descent method to increase the on-line learning capability of the RWNN. From the experimental results, the control performance of the proposed NHRWNN control system is more suitable than that of PI and PID controllers for a PMSM-driven electric scooter.

Acknowledgments

The author would like to acknowledge the financial support of the National Science Council of Taiwan, R.O.C., through its grant NSC 99-2221-E-239-040-MY3.

Nomenclature

v_{d1}, v_{q1}	d-axis and q-axis stator voltages
i_{d1}, i_{q1}	d-axis and q-axis stator currents
L_{d1}, L_{q1}	d-axis and q-axis stator inductances
R_1	stator resistance
$\omega_1^*, \omega, \omega_1$	command rotor angular speed, desired command rotor angular speed, rotor angular speed
P_1	number of poles
T_{L1}	load torque (external load disturbance, e.g., electric scooter)
B_1	viscous frictional coefficient
J_1	moment of inertia
λ_d	d-axis flux linkage
L_{m1}	mutual inductance
I_{fd1}	d-axis magnetizing current
T_m	electromagnet torque
K_e	torque constant
i_{q1}^*	q-axis command current
A_H, B_H, C_H	constants
$L_1^U(\omega_1)$	known continuous function
$\theta_f, \theta_1^*, \theta_1$	rotor flux position, command rotor position, rotor position
L_2^U, L_3	known constants
e_1	tracking error
U_H, U_H^*	control law, ideal control law
k_a	positive constants
U_{1S}, U_{2R}, U_{3C}	supervised control, recurrent wavelet neural network control, compensated control

V_1, V_2	Lyapunov functions
$\bar{V}_1$	positive constant
$\Omega(t)$	negative derivative of Lyapunov function
$c_i^1, c_i^2, c_j^3, c_k^4$	inputs of nodes in the input layer, mother wavelet layer, wavelet layer, output layer of the recurrent wavelet neural network
$g_i^1, g_j^2, g_k^3, g_o^4$	activation functions in the input layer, mother wavelet layer, wavelet layer, output layer of the recurrent wavelet neural network
$nod_i^1, nod_j^2, nod_k^3, nod_o^4$	node functions in the input layer, mother wavelet layer, wavelet layer, output layer of the recurrent wavelet neural network
$d_i^1, d_j^2, d_k^3, d_o^4$	outputs of nodes in the input layer, mother wavelet layer, wavelet layer, output layer of the recurrent wavelet neural network
N	number of iterations
$\mathrm{sgn}(\cdot)$	sign function
a_{ij}, b_{ij}	translations and dilations
$\mu_{jk}^3, \mu_{ko}^4, \mu_{oi}$	connective weights between the mother wavelet layer and the wavelet layer, connective weights between the wavelet layer and the output layer, recurrent weights for the units in the output layer
n, l_1	total number of the wavelets with respect to the input nodes, number of wavelets if each input node has the same mother wavelet nodes
$\partial V_2/\partial U_{2R}$	Jacobian term of controlled system
$\theta(x)$	first derivative of the Gaussian wavelet function
ψ	collection vector of the adjustable parameters of recurrent wavelet neural network
χ	input vector of the output layer of the recurrent wavelet neural network
σ	minimum approximation error
ψ^*	optimal weight vector that achieves the minimum approximation error
$\upsilon_j^2, \upsilon_k^3$	error term of mother wavelet function, error term of mother layer
α, β	small positive constant and adaptation gain
$\dot{\psi}$	adaptation laws of the recurrent wavelet neural network
i_{a1}^*, i_{b1}^*	command current in phase *a1*, command current in phase *b1*
i_{a1}, i_{b1}	measure current in phase *a1*, measure current in phase *b1*

References

[1] D.W. Novotny, T.A. Lipo, Vector Control and Dynamics of AC Drives, New York, Oxford University Press, 1996.

[2] W. Leonhard, Control of Electrical Drives, Berlin, Springer-Verlag, 1996.

[3] F.J. Lin, "Real-time IP position controller design with torque feedforward control for PM synchronous motor", IEEE Transactions on Industrial Electronics, Vol. 4, pp. 398–407, 1997.

[4] K.S. Narendra, K. Parthasarathy, "Identification and control of dynamical system using neural networks", IEEE Transactions on Neural Networks, Vol. 1, pp. 4–27, 1990.

[5] Y.M. Park, M.S. Choi, K.Y. Lee, "An optimal tracking neuro-controller for nonlinear dynamic systems", IEEE Transactions on Neural Networks, Vol. 7, pp. 1099–1110, 1996.

[6] F.F.M. El-Sousy, "A vector-controlled PMSM drive with a continually on-line learning hybrid neural-network model-following speed controller", Journal of Power Electronics, Vol. 5, pp. 197–210, 2005.

[7] C.H. Lin, "Switched reluctance motor drive for electric motorcycle using HFNN controller", 7th International Conference on Power Electronics and Drive Systems, pp. 1383–1388, 2007.

[8] S.S. Ge, C. Yang, T.H. Lee, "Adaptive predictive control using neural network for a class of pure-feedback systems in discrete time", IEEE Transactions on Neural Networks, Vol. 19, pp. 1599–1614, 2008.

[9] M. Ghariani, I.B. Salah, M. Ayadi, R. Neji, "Neural induction machine observer for electric vehicle applications", International Review of Electrical Engineering, Vol. 3, pp. 314–324, 2010.

[10] P. Brandstetter, M. Kuchar, I. Neborak , "Selected applications of artificial neural networks in the control of AC induction motor drives", International Review of Electrical Engineering, Vol. 4, pp. 1084–1093, 2011.

[11] Q. Zhang, A. Benveniste, "Wavelet networks", IEEE Transactions on Neural Networks, Vol. 3, pp. 889–898, 1992.

[12] B. Delyon, A. Juditsky, A. Benveniste, "Accuracy analysis for wavelet approximations", IEEE Transactions on Neural Networks, Vol. 6, pp. 332–348, 1995.

[13] J. Zhang, G.G. Walter, Y. Miao, W.N.W. Lee, "Wavelet neural networks for function learning", IEEE Transactions on Signal Processing, Vol. 43, pp. 1485–1496, 1995.

[14] J. Xu, D. W.C. Ho, D. Zhou, "Adaptive wavelet networks for nonlinear system identification", Proceedings of the American Control Conference, pp. 3472–3473, 1997.

[15] C.F. Chen, C.H. Hsiao, "Wavelet approach to optimizing dynamic systems", IEE Proceedings on Control Theory and Applications, Vol. 146, pp. 213–219, 1999.

[16] N. Sureshbabu, J.A. Farrell, "Wavelet-based system identification for nonlinear control", IEEE Transactions on Automatic Control, Vol. 44, pp. 412–417, 1999.

[17] Z. Zhang, C. Zhao, "A fast learning algorithm for wavelet network and its application in control", Proceedings of IEEE International Conference on Control Automation, pp. 1403–1407, 2007.

[18] S.A. Billings, H.L. Wei, "A new class of wavelet networks for nonlinear system identification", IEEE Transactions on Neural Networks, Vol. 16, pp. 862–874, 2005.

[19] D. Giaouris, J.W. Finch, O.C. Ferreira, R.M. Kennel, G.M. El-Murr, "Wavelet denoising for electric drives", IEEE Transactions on Industrial Electronics, Vol. 55, pp. 543–550, 2008.

[20] R.H. Abiyev, O. Kaynak, "Fuzzy wavelet neural networks for identification and control of dynamic plants—a novel structure and a comparative study", IEEE Transactions on Industrial Electronics, Vol. 55, pp. 3133–3140, 2008.

[21] D. Gonzalez, J.T. Bialasiewicz, J.Balcells, J. Gago, "Wavelet-based performance evaluation of power converters operating with modulated switching frequency", IEEE Transactions on Industrial Electronics, Vol. 55, pp. 3167–3176, 2008.

[22] F.J. Lin, R.J. Wai, M.P. Chen, "Wavelet neural network control for linear ultrasonic motor drive via adaptive sliding-mode technique", IEEE Transactions on Ultrasonics, Ferroelectrics, and Frequency Control, Vol. 50, pp. 686–697, 2003.

[23] S.H. Ling, H.H.C. Iu, F.H.F. Leung, K.Y. Chan, "Improved hybrid particle swarm optimized wavelet neural network for modeling the development of fluid dispensing for electronic packaging", IEEE Transactions on Industrial Electronics, Vol. 55, pp. 3447–3460, 2008.

[24] G. Gökmen, "Wavelet based instantaneous reactive power calculation method and a power system application sample", International Review of Electrical Engineering, Vol. 4, pp. 745–752, 2011.

[25] K. Funahashi, Y. Nakamura, "Approximation of dynamical systems by continuous time recurrent neural network", Neural Networks, Vol. 6, pp. 801–806, 1993.

[26] L. Jin, P.N. Nikiforuk, M. Gupta, "Approximation of discrete-time state-space trajectories using dynamic recurrent networks", IEEE Transactions on Automatic Control, Vol. 6, pp. 1266–1270, 1995.

[27] C.C. Ku, K.Y. Lee, "Diagonal recurrent neural networks for dynamical system control", IEEE Transactions on Neural Networks, Vol. 6, pp. 144–156, 1995.

[28] F.J. Lin, R.J. Wai, C.M. Hong, "Hybrid supervisory control using recurrent fuzzy neural network for tracking periodic inputs", IEEE Transactions on Neural Networks, Vol. 12, pp. 68–90, 2001.

[29] C.H. Lu, C.C. Tsai, "Adaptive predictive control with recurrent neural network for industrial processes: an application to temperature control of a variable-frequency oil-cooling machine", IEEE Transactions on Industrial Electronics, Vol. 55, pp. 1366–1375, 2008.

[30] S.J. Yoo, J.B. Park, Y.H. Choi, "Stable predictive control of chaotic systems using self-recurrent wavelet neural network", International Journal of Automatic Control Systems, Vol. 3, pp. 43–55, 2005.

[31] C.H. Lu, "Design and application of stable predictive controller using recurrent wavelet neural networks", IEEE Transactions on Industrial Electronics, Vol. 56, pp. 3733–3742, 2009.

[32] C.H. Lin, C.P. Lin, "The hybrid RFNN control for a PMSM drive system using rotor flux estimator", International Conference on Power Electronics and Drive Systems, pp. 1394–1399, 2009.

[33] C.H. Lin, P.H. Chiang, C.S. Tseng, Y.L. Lin, M.Y. Lee, "Hybrid recurrent fuzzy neural network control for permanent magnet synchronous motor applied in electric scooter", International Power Electronics, pp. 1371–1376, 2010.

[34] J.J.E. Slotine, W. Li, Applied Nonlinear Control, Englewood Cliffs, NJ, USA, Prentice Hall, 1991.

[35] K.J. Astrom, B. Wittenmark, Adaptive Control, New York, Addison-Wesley, 1995.

[36] Y.Oussar, G. Dreyfus, "Initialization by selection for wavelet network training", Neurocomputing, Vol. 34, pp. 131–143, 2000.